

A simple way to improved formulation of FE^2 analysis

Urša Šolinc¹ · Jože Korelc¹

Received: 2 July 2015 / Accepted: 12 August 2015 / Published online: 5 October 2015
© Springer-Verlag Berlin Heidelberg 2015

Abstract A new formulation of two-scale FE^2 analysis introduces symmetric stretch tensor as strain measure on macro level instead of asymmetric deformation gradient to determine boundary conditions on embedded microstructure. This significantly reduces computational cost of boundary conditions related sensitivity analysis of microstructure and with it the evaluation of local macroscopic stress tensors and tangent matrices. Various FE^2 formulations with isogeometric and standard finite element microanalysis are tested for consistency, accuracy and numerical efficiency on numerical homogenisation examples. Objective performance comparison of different FE^2 formulations is enabled with automation of all procedures in symbolic code generation system AceGen. The results obtained in numerical examples show reduced computational cost of the new FE^2 formulation without loss of accuracy and comparable numerical efficiency of higher order isogeometric and standard FE^2 formulations.

Keywords Optimized multiscale formulation · Automatic code generation · Multiscale method · Numerical homogenisation

1 Introduction

A two-scale FE^2 scheme is a well established computational homogenisation technique [1–7] for determination of

material characteristics of multiphase materials. FE^2 method predicts the global response of microscopic heterogeneous materials (such as metal alloy systems, polymer blends, porous media, polycrystalline materials and composites) by employing micromechanical models and transferring the microscale information to the macroscale analysis. The computational cost of FE^2 analysis is enormous since this nested finite element method framework simultaneously analyzes microstructure and macrostructure. This paper presents a new FE^2 formulation with reduced computational cost without altering the numerical model of multiphase material. At each Newton–Raphson iteration on macro level local tangent operator consistent with local macroscopic stress tensor is extracted from embedded microscale computation. A conventional way is based on the idea of condensing the microscale tangent information stored in the global finite element tangent matrix to a fourth-order local tangent operator at macroscopic integration point (see [2]). In case of complex microstructures this procedure inflicts too high memory allocation demands for standard workstations to handle (see [8,9]). An alternative technique for tangent computation was presented by Lamut (see [8]) which determines local macroscopic tangent operator with sensitivity analysis of embedded microstructure with respect to boundary conditions (see [10]). Result of sensitivity analysis are partial derivatives of response function with respect to sensitivity parameters, which are independent components of the macro strain measure. Macro strain measure is in a conventional FE^2 procedure asymmetric macroscopic deformation gradient with nine independent components. A motivation for this paper was to reduce computational cost of sensitivity analysis with transition to symmetric stretch tensor as macro strain measure which reduces the number of sensitivity parameters from nine to six. For this study also various FE^2 formulations with isogeometric and standard finite element

✉ Jože Korelc
jkorelc@fgg.uni-lj.si
Urša Šolinc
ursa.solinc@fgg.uni-lj.si

¹ Faculty of Civil and Geodetic Engineering, University of Ljubljana, Jamova 2, 1000 Ljubljana, Slovenia

microanalysis were developed and compared on numerical homogenisation examples. To enable objective performance comparison of different FE² formulations are all considered procedures implemented in automatic code generator Ace-Gen which provides uniformly automated FE² flowchart. Different FE² formulations are tested for consistency of micro–macro coupling, accuracy and numerical efficiency on numerical homogenisation examples with hyperelastic and linear elastic porous material. For accuracy validation in linear case a Nemat-Nassers analytical estimate of effective elastic tensor is calculated (see [11–13]) and compared to numerical solution. Findings of this study are summarized in conclusions at the end of this paper.

2 Specifics of proposed approach to FE² method

FE² homogenisation scheme simultaneously analyses heterogeneous multi-phase material on two nested scales of finite elements. On the outer loop of FE² procedure macrostructure is analyzed and discretized with finite elements. To each macroscopic integration point a representative volume element (RVE) is assigned, which represents the underlying microstructure. This research deals with hyperelastic multiphase materials and assumes that constitutive behavior of all microstructural constituents is known and defined by strain energy function. Contrary to conventional formulation which determines prescribed essential boundary conditions on RVE with local macroscopic deformation gradient \mathbf{F}_M (see [2]) this paper presents transition to symmetric tensor with the aim of reducing the computational cost of local macroscopic tangent matrix evaluation. The right polar decomposition of the deformation gradient \mathbf{F}_M into a product of an orthogonal tensor \mathbf{R}_M and a positive definite symmetric tensor \mathbf{U}_M (see [14]), is written as

$$\mathbf{F}_M = \mathbf{R}_M \cdot \mathbf{U}_M, \quad (1)$$

where \mathbf{R}_M represents rigid rotation and \mathbf{U}_M the stretch tensor. Here and in the following the subscript “M” refers to macroscale quantity, while the subscript “m” will denote a microscopic quantity. The material characteristics of hyperelastic material depend only on stretch tensor \mathbf{U}_M , since rigid body rotation does not alter the material volume or shape. Since local macroscopic Cauchy–Green tensor $\mathbf{C}_M = \mathbf{F}_M^T \mathbf{F}_M = \mathbf{U}_M \mathbf{U}_M$ is symmetric and positive definite, \mathbf{U}_M is unique symmetric positive definite square root of \mathbf{C}_M . The exact finite term expansion of matrix square root and its first and second derivative was obtained by differentiating a scalar generating function of the eigenvalues of \mathbf{C}_M (see [15]) as

$$\mathbf{U}_M = \frac{2}{3} \frac{\partial \left(E_1^{3/2} + E_2^{3/2} + E_3^{3/2} \right)}{\partial \mathbf{C}_M}, \quad (2)$$

where E_1, E_2, E_3 are eigenvalues of \mathbf{C}_M determined with trigonometric functions (see [16,17]). In case of multiple or almost equal eigenvalues in which general formulation exhibits ill-conditioning, asymptotic expansions presented in [17] are applied. The actual derivatives were obtained with use of backward mode automatic differentiation technique as described in [17]. In this way the usual evaluation of matrix square root function based on polar decomposition and associated numerical difficulties are avoided. Hence, prescribed boundary conditions can be formulated with \mathbf{U}_M instead of \mathbf{F}_M without prejudice to the generality of FE² method.

RVE is brick shaped and essential boundary conditions are assigned in each corner node on the RVE boundary as

$$\bar{\mathbf{u}} = (\mathbf{U}_M - \mathbf{I}) \mathbf{B}_c, \quad (3)$$

where \mathbf{B}_c are reference coordinates of a corner node in RVE. For the unconstrained boundary nodes microstructural periodicity assumption is adopted as justified by a number of authors [2,9,18]. The deformed position of all unconstrained nodes on RVE boundary is constrained with periodicity conditions written in general form as

$$\mathbf{x}^+ - \mathbf{x}^- = \mathbf{U}_M (\mathbf{X}^+ - \mathbf{X}^-) = \mathbf{U}_M (\mathbf{B}_c^+ - \mathbf{B}_c^-), \quad (4)$$

where \mathbf{x}^+ and \mathbf{x}^- (\mathbf{X}^+ and \mathbf{X}^-) denote deformed (reference) position of nodes on opposite RVE boundary surfaces and \mathbf{B}_c^+ and \mathbf{B}_c^- represent reference position of associated corner nodes. Periodic boundary conditions in (4) imply periodic deformation and stress field (see [11]). Thus, for boundary stress $\mathbf{p} = \mathbf{P}_m \cdot \mathbf{n}$, where \mathbf{P}_m is the microscopic 1. Piola–Kirchhoff stress tensor and \mathbf{n} is the associated normal to the undeformed RVE boundary surface it holds true that $\mathbf{p}^+ = \mathbf{p}^-$ on opposite boundary surfaces of RVE. Periodicity conditions (4) are added to microscale analysis as equality constraints for a given boundary problem which is then solved monolithically with the method of Lagrange multipliers. On the inner loop of FE² analysis RVE is discretized and analyzed with finite elements. Additional Lagrange finite elements link displacements of the constrained corner nodes \mathbf{B}_c with those of unconstrained nodes on opposing boundary planes of RVE. The Lagrange finite elements are defined by augmented Lagrange multiplier potential,

$$\mathcal{E}(\lambda_i) = \lambda_i (\mathbf{u}^+ - \mathbf{u}^-) + \rho (\mathbf{u}^+ - \mathbf{u}^-)^2, \quad (5)$$

where $\lambda_i = \{\lambda_1, \lambda_2, \lambda_3\}$ are the Lagrange multipliers of the i -th equality constraint and ρ is arbitrary weight.

3 The proof of consistency of micro - macro coupling

The coupling between macroscopic and microscopic levels is based on averaging theorems [11, 19, 20]. The energy averaging theorem known as Hill–Mandel condition requires equality between volume average of virtual work performed by variation of microscopic deformations on RVE and virtual work performed by variation of macroscopic deformations in associated point on macro-scale,

$$\frac{1}{V_0} \int_{V_0} \mathbf{P}_m : \delta \mathbf{F}_m^T dV = \mathbf{P}_M : \delta \mathbf{F}_M^T, \quad \forall \delta \mathbf{x}, \quad (6)$$

where \mathbf{P}_M is the 1st Piola–Krichhoff stress tensor associated with variation of work conjugate deformation gradient $\delta \mathbf{F}_M$. Here it will be shown that the equality (6) holds true also in the case where only symmetric stretch tensor \mathbf{U}_M defines boundary conditions on RVE without the rotational part \mathbf{R}_M of the polar decomposition of deformation gradient \mathbf{F}_M . The volume average of microstructural deformation gradient \mathbf{F}_m over RVE in case of periodic boundary conditions (4) equals

$$\begin{aligned} \frac{1}{V_0} \int_{V_0} \mathbf{F}_m dV &= \frac{1}{V_0} \int_{V_0} (\nabla \mathbf{x})^T dV = \frac{1}{V_0} \int_{\Gamma_0} \mathbf{x} \mathbf{n} d\Gamma \\ &= \frac{1}{V_0} \int_{\Gamma_0^+} (\mathbf{x}^+ - \mathbf{x}^-) \mathbf{n}^+ d\Gamma \\ &= \frac{1}{V_0} \mathbf{U}^M \cdot \int_{\Gamma_0^+} (\mathbf{X}^+ - \mathbf{X}^-) \mathbf{n}^+ d\Gamma \\ &= \frac{1}{V_0} \mathbf{U}^M \cdot \int_{\Gamma_0} \mathbf{X} \mathbf{n} d\Gamma \\ &= \frac{1}{V_0} \mathbf{U}^M \cdot \int_{V_0} \nabla \mathbf{X} dV = \mathbf{U}^M, \end{aligned} \quad (7)$$

where equality $\nabla \mathbf{X} = \mathbf{I}$ is taken into account and divergence theorem is used to transform the integral over undeformed volume V_0 of the RVE to an integral over undeformed boundary surface Γ_0 of the RVE with associated normal \mathbf{n} and vice versa. This yields the relation between macroscopic deformation gradient \mathbf{F}_M and the volume average of its microstructural counterpart \mathbf{F}_m as

$$\mathbf{F}_M = \mathbf{R}_M \cdot \mathbf{U}_M = \mathbf{R}_M \cdot \frac{1}{V_0} \int_{V_0} \mathbf{F}_m dV. \quad (8)$$

Volume average of microstructural 1. Piola–Kirchhoff stress tensor \mathbf{P}_m resulting from boundary conditions (4) on RVE, equals

$$\hat{\mathbf{P}} = \frac{1}{V_0} \int_{V_0} \mathbf{P}_m dV. \quad (9)$$

Macroscopic 1. Piola–Kirchhoff stress tensor \mathbf{P}_M is obtained after the rotation tensor \mathbf{R}_M is superimposed upon deformed form caused by stretch tensor \mathbf{U}_M , affecting the direction of stress field and leading to relation

$$\mathbf{P}_M = \mathbf{R}_M \cdot \hat{\mathbf{P}}. \quad (10)$$

When the right side of Hill–Mandel condition (6), $\mathbf{P}_M : \delta \mathbf{F}_M$, is expressed in terms of Biot stress tensor \mathbf{T}_M and its work conjugate pair, the stretch tensor \mathbf{U}_M , it can be seen that

$$\begin{aligned} \mathbf{P}_M : \delta \mathbf{F}_M^T &= \mathbf{T}_M : \delta \mathbf{U}_M \\ &= \frac{1}{2} (\mathbf{R}_M^T \mathbf{P}_M + \mathbf{P}_M^T \mathbf{R}_M) : \delta \mathbf{U}_M \\ &= \frac{1}{2} (\mathbf{R}_M^T \mathbf{R}_M \hat{\mathbf{P}} + (\mathbf{R}_M \hat{\mathbf{P}})^T \mathbf{R}_M) : \delta \mathbf{U}_M \\ &= \frac{1}{2} (\hat{\mathbf{P}} + \hat{\mathbf{P}}^T) : \delta \mathbf{U}_M \\ &= \hat{\mathbf{P}} : \delta \mathbf{U}_M, \end{aligned} \quad (11)$$

since $\hat{\mathbf{P}} : \delta \mathbf{U}_M = \text{tr}(\hat{\mathbf{P}}^T \delta \mathbf{U}_M) = \text{tr}(\hat{\mathbf{P}} \delta \mathbf{U}_M) = \hat{\mathbf{P}}^T : \delta \mathbf{U}_M$ and \mathbf{R}_M is orthogonal tensor, thus $\mathbf{R}_M^T \mathbf{R}_M = \mathbf{I}$. When periodicity conditions (4) on RVE boundary Γ_0 are applied to the left side of the Hill–Mandel equality (6) and divergence theorem is put into use it can be expressed as

$$\begin{aligned} \frac{1}{V_0} \int_{V_0} \mathbf{P}_m : \delta \mathbf{F}_m^T dV &= \frac{1}{V_0} \int_{\Gamma_0} \mathbf{p} \cdot \delta \mathbf{x} d\Gamma \\ &= \frac{1}{V_0} \int_{\Gamma_0^+} \mathbf{p}^+ (\mathbf{X}^+ - \mathbf{X}^-) d\Gamma : \delta \mathbf{U}_M \\ &= \frac{1}{V_0} \int_{\Gamma_0} \mathbf{p} \mathbf{X} d\Gamma : \delta \mathbf{U}_M \\ &= \frac{1}{V_0} \int_{V_0} \mathbf{P}_m dV : \delta \mathbf{U}_M = \hat{\mathbf{P}} : \delta \mathbf{U}_M, \end{aligned} \quad (12)$$

where $\mathbf{p} = \mathbf{P}_m \cdot \mathbf{n}$ (for more details see [21]). This proves the equality of the left and the right side of the Hill–Mandel macrohomogeneity condition (6) for chosen boundary conditions (4).

4 Automatic differentiation based (ADB) notation

Multiscale FE² procedure is implemented in symbolic code generation system AceGen that combines the symbolic and algebraic capabilities of general computer algebra system Mathematica [22], automatic differentiation technique and simultaneous optimization of expressions (see [23, 24]). ADB method [25–27] is used for evaluation of the exact derivatives of any arbitrary complex function via chain rule and represents an alternative solution to the numerical

differentiation and symbolic differentiation. ADB operator $\hat{\delta} f(\mathbf{a})/\hat{\delta} \mathbf{a}$ represents partial differentiation of a function $f(\mathbf{a})$ with respect to variables \mathbf{a} . If for example an alternative or additional dependencies for variables \mathbf{b} have to be considered for differentiation, local ADB exception is indicated by the following formalism:

$$\frac{\hat{\delta} f(\mathbf{a}, \mathbf{b})}{\hat{\delta} \mathbf{a}} \Bigg|_{\frac{D\mathbf{b}}{D\mathbf{a}}=\mathbf{M}}, \tag{13}$$

which indicates that during ADB procedure, the total derivatives of variables \mathbf{b} with respect to variables \mathbf{a} are set to be equal to matrix \mathbf{M} . The ADB notation can be directly translated in the program code and is part of numerically efficient code automation. Further details regarding this notation can be found in [10].

5 Numerical formulation of proposed approach to FE² method

The response of each phase in heterogeneous RVE is defined by constitutive equation specified with a strain energy function $\Psi(\mathbf{F}_m)$. The neo-Hookean type of strain energy function used in numerical examples in Sect. 7 is chosen in a form

$$\Psi(\mathbf{F}_m) = \frac{\mu}{2} \left(J_F^{-2/3} \text{tr}(\mathbf{C}_m) - 3 \right) + \frac{K}{\beta^2} \left(J_F^{-\beta} - 1 + \beta \ln(J_F - 3) \right), \tag{14}$$

where \mathbf{C}_m is Cauchy–Green deformation tensor, $J_F = \det \mathbf{F}_m$, μ is shear modulus, K is compression modulus and β is dimensionless parameter. In RVE analysis is augmented Lagrange multiplier potential \mathcal{E} defined in (5) added to elastic deformation energy $\int_{V_0} \Psi dV$, yielding in the absence of external forces the system of nonlinear equations

$$\mathbf{R}_m = \frac{\partial}{\partial \mathbf{p}} \left(\mathcal{E}(\mathbf{p}) + \int_{V_0} \Psi(\mathbf{F}_m) dV \right) = \mathbf{0}, \quad \text{where} \tag{15}$$

$$\mathbf{p} = \mathbf{u} \cup \boldsymbol{\lambda},$$

\mathbf{p} is a vector of unknowns composed of nodal displacements \mathbf{u} and Lagrange multipliers $\boldsymbol{\lambda}$. Global residual vector \mathbf{R}_m of micro problem assembled through integration domains as

$$\mathbf{R}_m = \mathbf{A} \mathbf{R}_{le} + \mathbf{A} \sum_{e=1}^{n_e} \sum_{g=1}^{n_g} w_{mg} J_{mg} \mathbf{R}_{mg}, \tag{16}$$

where operator \mathbf{A} stands for standard FE assembly procedure through finite element domains e and Lagrange element domains le , $\mathbf{R}_{le} = \hat{\delta} \mathcal{E} / \hat{\delta} \mathbf{p}_{le}$ is Lagrange element residual, g

is Gauss point and w_{mg} , J_{mg} , $\mathbf{R}_{mg} = \hat{\delta} \Psi / \hat{\delta} \mathbf{p}_e$ are the corresponding Gauss point weight, Jacobian determinant and residual, respectively. System of equations (15) is solved numerically with standard Newton–Raphson method. The resulting microstress field is expressed as 1st Piola-Kirchhoff stress tensor $\mathbf{P}_m = \partial \Psi(\mathbf{F}_m) / \partial \mathbf{F}_m$, averaged over RVE volume and returned to macroscopic integration point as local macroscopic stress $\hat{\mathbf{P}}$,

$$\hat{\mathbf{P}} = \frac{1}{V_0} \sum_{e=1}^{n_e} \sum_{g=1}^{n_g} w_{mg} J_{mg} \mathbf{P}_{mg}, \tag{17}$$

where V_0 is RVE volume and $\mathbf{P}_{mg} = \hat{\delta} \Psi / \hat{\delta} \mathbf{F}_m$ is Gauss point stress tensor. Macroelement formulation is established in terms of a weak statement of static equilibrium of the body. Contribution of internal forces to global weak form is given as:

$$\delta W_{\text{int}} = \int_{V_M} \mathbf{P}_M : \delta \mathbf{F}_M^T dV = \int_{V_M} \hat{\mathbf{P}} : \delta \mathbf{U}_M dV, \tag{18}$$

where δW_{int} is the internal virtual work done by the stresses and V_M is the volume of the body on macroscale (see [14]). The contribution of internal forces to residual of macro problem is obtained in the same manner as the residual of micro problem, i. e.

$$\mathbf{R}_M = \mathbf{A} \sum_{e=1}^{N_e} \sum_{g=1}^{N_g} w_{Mg} J_{Mg} \mathbf{R}_{Mg}, \tag{19}$$

where \mathbf{R}_{Mg} is Gauss point contribution given by

$$\mathbf{R}_{Mg} = \hat{\mathbf{P}} : \frac{\partial \mathbf{U}_M}{\partial \mathbf{u}_e} = \frac{\hat{\delta}(\hat{\mathbf{P}} : \mathbf{U}_M)}{\hat{\delta} \mathbf{u}_e} \Bigg|_{\frac{D\hat{\mathbf{P}}}{D\mathbf{u}_e}=\mathbf{0}}. \tag{20}$$

The requirement that global residual be zero yields nonlinear system of equations which is solved numerically with standard Newton–Raphson method. Like global residual is macroscopic tangent operator \mathbf{K}_M formed from Gauss point tangent operator \mathbf{K}_{Mg} which is obtained via chain rule as

$$\mathbf{K}_{Mg} = \frac{\partial \mathbf{R}_{Mg}}{\partial \mathbf{u}_e} + \frac{\partial \mathbf{R}_{Mg}}{\partial \hat{\mathbf{P}}} \frac{D\hat{\mathbf{P}}}{DU_M} \frac{\partial \mathbf{U}_M}{\partial \mathbf{u}_e} = \frac{\hat{\delta} \mathbf{R}_{Mg}}{\hat{\delta} \mathbf{u}_e} \Bigg|_{\frac{D\hat{\mathbf{P}}}{DU_M}=D\hat{\mathbf{P}}DU_M}. \tag{21}$$

The first derivative $D\hat{\mathbf{P}}/DU_M$ of average stress tensor $\hat{\mathbf{P}}$ with respect to symmetric stretch tensor \mathbf{U}_M in (21) is obtained from boundary conditions related sensitivity analysis of the microstructure (RVE).

5.1 Sensitivity analysis on RVE

Macroscopic stress tensor $\hat{\mathbf{P}}$ is defined as averaged microstress over volume of the RVE (see (9)) so the total derivative $D\hat{\mathbf{P}}/DU_M$ can be written as

$$\frac{D\hat{\mathbf{P}}}{DU_M} = \frac{1}{V_0} \int_{V_0} \frac{D\mathbf{P}_m}{DU_M} dV. \tag{22}$$

and evaluated on micro level as averaged sensitivity of microscopic 1. Piola-Kirchhoff stress tensor \mathbf{P}_m on variation of sensitivity parameters, which are defined as the six independent components of the symmetric tensor \mathbf{U}_M ,

$$\boldsymbol{\phi} = \{U_{11}, U_{12}, U_{13}, U_{22}, U_{23}, U_{33}\}. \tag{23}$$

Sensitivity problem is in analogy with primal analysis defined by residual \mathbf{R}_m ,

$$\mathbf{R}_m(\mathbf{p}(\boldsymbol{\phi}), \bar{\mathbf{u}}(\boldsymbol{\phi})) = \mathbf{0}, \tag{24}$$

where $\bar{\mathbf{u}}$ are prescribed essential boundary conditions and \mathbf{p} is a vector of unknowns all defined as a function of sensitivity parameters $\boldsymbol{\phi}$. The direct differentiation of time-independent residual (24) with respect to sensitivity parameters $\boldsymbol{\phi}$ yields the following system of linear equations for response sensitivity $D\mathbf{p}/D\boldsymbol{\phi}$,

$$\frac{\partial \mathbf{R}_m}{\partial \mathbf{p}} \frac{D\mathbf{p}}{D\boldsymbol{\phi}} = -\frac{\partial \mathbf{R}_m}{\partial \bar{\mathbf{u}}} \frac{D\bar{\mathbf{u}}}{D\boldsymbol{\phi}}, \tag{25}$$

where $\partial \mathbf{R}_m/\partial \mathbf{p}$ is exactly the independent tangent operator \mathbf{K}_m of the primal problem on micro level. The global sensitivity problem is then rewritten as

$$\mathbf{K}_m \frac{D\mathbf{p}}{D\boldsymbol{\phi}} = -\tilde{\mathbf{R}}_m, \tag{26}$$

where $\tilde{\mathbf{R}}_m$ is sensitivity pseudo residual formed from Gauss point pseudo residual $\tilde{\mathbf{R}}_{mg}$ and Lagrange element pseudo residual $\tilde{\mathbf{R}}_{le}$ defined by

$$\tilde{\mathbf{R}}_{mg} = \left. \frac{\hat{\mathbf{R}}_{mg}}{\hat{\boldsymbol{\phi}}} \right|_{\frac{D\bar{\mathbf{u}}}{D\boldsymbol{\phi}}=D\bar{\mathbf{u}}D\boldsymbol{\phi}} \quad \text{and} \quad \tilde{\mathbf{R}}_{le} = \left. \frac{\hat{\mathbf{R}}_{le}}{\hat{\boldsymbol{\phi}}} \right|_{\frac{D\bar{\mathbf{u}}}{D\boldsymbol{\phi}}=D\bar{\mathbf{u}}D\boldsymbol{\phi}}, \tag{27}$$

respectively, where $D\bar{\mathbf{u}}D\boldsymbol{\phi}$ is boundary condition velocity field. $D\bar{\mathbf{u}}D\boldsymbol{\phi}$ represents the derivatives of prescribed essential boundary conditions $\bar{\mathbf{u}}$ with respect to sensitivity parameters $\boldsymbol{\phi}$ which is input data for microanalysis. Sensitivity problem (26) is solved after converged solution for

primal problem is obtained. Then the average stress sensitivity $D\hat{\mathbf{P}}/DU_M$ is calculated with direct differentiation as

$$\frac{D\hat{\mathbf{P}}}{DU_M} = \frac{1}{V_0} \sum_{e=1}^{n_e} \sum_{g=1}^{n_g} w_{mg} J_{mg} \left. \frac{\hat{\mathbf{P}}_{mg}}{\hat{\boldsymbol{\phi}}} \right|_{\frac{D\mathbf{p}_e}{D\boldsymbol{\phi}}=D\mathbf{p}D\boldsymbol{\phi}}, \tag{28}$$

where $D\mathbf{p}D\boldsymbol{\phi}$ is the result of sensitivity analysis.

6 Automation of FE² procedure

A pseudocode of automated displacement based FE² analysis is given in Algorithm 1 for the analysis on macro level and in Algorithm 2 for microanalysis. Flowchart for macroelement is applicable on arbitrary finite element formulated on virtual work principle as presented in Sect. 5. Local macroscopic stretch tensor \mathbf{U}_M determines essential boundary conditions on associated RVE (see (3), (4)). Lagrange finite elements are introduced to impose periodicity constraints on displacements of nodes on RVE boundary. Primal analysis of RVE is in Algorithm 2 augmented with boundary conditions related sensitivity analysis as explained in 5.1. Sensitivity of prescribed boundary conditions on variation of \mathbf{U}_M is defined on the input. When static equilibrium is achieved under given equality constraints, microanalysis returns to the macroscopic integration point average stress tensor $\hat{\mathbf{P}}$ and its sensitivity $D\hat{\mathbf{P}}DU_M$ on variation of \mathbf{U}_M . Convergence of the iterative Newton–Raphson method has to be achieved simultaneously on micro and macro level on each load step for the overall convergence of the FE² method.

Algorithm 1: FE² analysis - macro level

```

Input: Position of macrostructural nodal points B
Input: Starting value for nodal displacements  $\mathbf{u}_0$ , parameter increment  $\Delta\lambda$ 
 $\lambda \leftarrow 0; \mathbf{u} \leftarrow \mathbf{u}_0;$ 
repeat
   $\lambda \leftarrow \lambda + \Delta\lambda$ 
  begin iterative solution of one step of primal analysis on macro level
    repeat
      foreach macro element do
        foreach Gauss point  $g$  do
           $\mathbf{X} \leftarrow \mathbf{N}_a \cdot \mathbf{B}_e;$  //  $\mathbf{N}_a$  are shape functions
           $\mathbf{u}_e \leftarrow \mathbf{N}_a \cdot \mathbf{u}_e;$ 
           $\mathbf{J}_e \leftarrow \frac{\delta \mathbf{X}}{\delta \boldsymbol{\xi}}; \mathbf{H} \leftarrow \frac{\delta \mathbf{u}_e}{\delta \mathbf{X}} \Big|_{\frac{D\boldsymbol{\xi}}{D\mathbf{X}}=\mathbf{J}_e^{-1}}; J_g \leftarrow \det \mathbf{J}_e;$ 
           $\mathbf{F}_M \leftarrow \mathbf{H} + \mathbf{I}; \mathbf{C}_M \leftarrow \mathbf{F}_M^T \mathbf{F}_M;$ 
           $\mathbf{U}_M \leftarrow \sqrt{\mathbf{C}_M};$ 
          begin solution of microanalysis
            procedure of microanalysis is presented in Algorithm 2 and it
            returns averaged stress tensor  $\hat{\mathbf{P}}$  and sensitivity  $D\hat{\mathbf{P}}DU_M$ 
           $\mathbf{W}_M \leftarrow \hat{\mathbf{P}} : \mathbf{U}_M;$  // Gauss point internal virtual work
           $\mathbf{R}_{Mg} \leftarrow \frac{\delta \mathbf{W}_M}{\delta \mathbf{u}_e} \Big|_{\frac{D\hat{\mathbf{P}}}{D\mathbf{u}_e}=0};$  // calculate Gauss point residual
          using ADB exception
           $\mathbf{K}_{Mg} \leftarrow \frac{\delta \mathbf{R}_{Mg}}{\delta \mathbf{u}_e} \Big|_{\frac{D\hat{\mathbf{P}}}{DU_M}=D\hat{\mathbf{P}}DU_M};$  // calculate Gauss point
          tangent matrix using ADB exception
          add  $w_g J_g \mathbf{R}_{Mg}$  to  $\mathbf{R}_{Me}$  and  $w_{Mg} J_{Mg} \mathbf{K}_{Mg}$  to  $\mathbf{K}_{Me}$ 
        end foreach
      assemble  $\mathbf{R}_{Me}$  to  $\mathbf{R}_M$  and  $\mathbf{K}_{Me}$  to  $\mathbf{K}_M$ 
    end foreach
    solve  $\mathbf{K}_M \Delta \mathbf{u} + \mathbf{R}_M = \mathbf{0}$  for unknown  $\Delta \mathbf{u}$ 
     $\mathbf{u} \leftarrow \mathbf{u} + \Delta \mathbf{u}$ 
  until error criterion for  $\|\mathbf{R}_M\|$  and  $\|\Delta \mathbf{u}\|$  is fulfilled;
until terminal value of parameter  $\lambda$  is reached;
Result:  $\mathbf{u}$  // converged solution in last step
    
```


Algorithm 2: FE² analysis - micro level

```

Input: Primal analysis: Material data ( $K, \mu$ ), position of microstructural nodal points,
prescribed displacements  $\bar{u}$  in RVE corner nodes  $B_c$  and other type of
information depending on the chosen finite element formulation
Input: Sensitivity analysis: sensitivity parameters  $\phi$ , boundary condition velocity field
 $D\bar{u}D\phi$ 
 $\bar{u} \leftarrow (U_M - \mathbf{I}) \cdot B_c$ ; // prescribed essential boundary conditions for
constrained nodes  $B_c$ 
begin solution of primal analysis
  procedures of primal analysis for different element formulations are collected in [10]
  hyperelastic potential  $W_m$  is a sum of strain energy function and Lagrange
  multiplier potential, see equation (16)
   $R_m \leftarrow \frac{\delta W_m}{\delta P}$ ;  $K_m \leftarrow \frac{\delta R_m}{\delta P}$ ; // calculate finite element residual and tangent
  matrix using ADB exception
begin solution of sensitivity problem
   $\phi \leftarrow \{U_{ij}; U_{ij} \in U_M \wedge i \leq j\}$ ; // set sensitivity parameters  $\phi$ 
   $D\bar{u}D\phi_k \leftarrow \{\frac{\partial \bar{u}}{\partial \phi_k}; \phi_k \in \phi\}$ ; // set boundary conditions velocity field
  foreach solid element do
    foreach Gauss point g do
       $\bar{R}_{mg} \leftarrow \{\frac{\delta R_{mg}}{\delta \phi_k} \mid \frac{D\bar{u}}{D\phi_k} = D\bar{u}D\phi_k; \phi_k \in \phi\}$ ; // calculate Gauss point
      pseudo residual using ADB exception
      add  $w_g J_g \bar{R}_{mg}$  to  $\bar{R}_{me}$ 
    end foreach
    assemble  $\bar{R}_{me}$  to  $\bar{R}_m$ 
  end foreach
  foreach Lagrange element do
     $\bar{R}_{le} \leftarrow \{\frac{\delta R_{le}}{\delta \phi_k} \mid \frac{D\bar{u}}{D\phi_k} = D\bar{u}D\phi_k; \phi_k \in \phi\}$ ; // calculate Lagrange element
    pseudo residual using ADB exception
    assemble  $\bar{R}_{le}$  to  $\bar{R}_m$ 
  end foreach
  solve  $K_m \frac{D\bar{P}}{D\phi} + \bar{R}_m = 0$  for unknown  $\frac{D\bar{P}}{D\phi}$  using already factorized  $K_m$  from
  primal analysis
begin evaluate microscopic stiffness and averaged stress over RVE volume  $V$ 
  foreach element in RVE do
    foreach Gauss point g do
       $P_{mg} \leftarrow \frac{\delta W_m}{\delta F_m}$ ; // Gauss point 1st Piola-Kirchhoff stress tensor
       $DP_{mg}DU_M \leftarrow \frac{\delta P_{mg}}{\delta \phi} \mid \frac{DP_{mg}}{D\phi_k} = DP_{mg}D\phi_k \forall k \in \{1, \dots, 6\}$ ;
      add  $w_{mg} J_{mg} DP_{mg}DU_M$  to  $DP_{me}DU_M$  and  $w_{mg} J_{mg} P_{mg}$  to  $P_{me}$ 
    end foreach
    add  $DP_{me}DU_M$  to  $DP_mDU_M$  and  $P_{me}$  to  $P_m$ 
  end foreach
  calculate averaged stress  $\bar{P} = \frac{1}{V_0} P_m$  and export  $\bar{P}$  to macroscopic Gauss point
  data
  calculate averaged tangent matrix  $D\bar{P}DU_M = \frac{1}{V_0} DP_mDU_M$  and export
   $D\bar{P}DU_M$  to macroscopic Gauss point data
Result:  $\bar{P}, D\bar{P}DU_M$ 

```

7 Accuracy and numerical efficiency of proposed FE² formulation

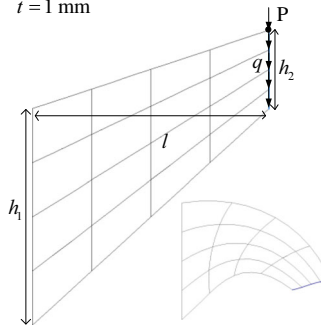
Various automated FE² formulations with isogeometric and standard finite element microanalysis are tested for consistency, accuracy and numerical efficiency consideration on chosen computational homogenisation examples. All numerical examples are performed with three-dimensional solid finite elements. Procedures of primal and sensitivity analyses shown in Algorithm 2 were obtained from [10]. Procedure of primal isogeometric analysis follows formulation presented in [28]. All calculations are executed without parallelization on 8 GB RAM and 2.8 GHz processor.

7.1 Test of consistency of micro–macro coupling

A test with homogeneous material was considered to show that the results of implemented FE² procedure are identical to those of single scale analysis in the case of homogeneous micro structure. A standard Cooke membrane is discretized with a mesh of $4 \times 1 \times 4$ standard linear Lagrange (H1) finite elements for single scale analysis and for macro level of two-

(A) MACROSCALE

Geometry Constraints
 $h_1 = 44 \text{ mm}$ $X = 0: u = v = 0$
 $h_2 = 16 \text{ mm}$ Load
 $l = 48 \text{ mm}$ $q = 1 \text{ MPa}$
 $t = 1 \text{ mm}$



(B) MICROSCALE

Material
 $K = 0.33333 \text{ MPa}$
 $\mu = 0.5 \text{ MPa}$
 $\beta = -2$
 Volume fraction of opening = 0.1

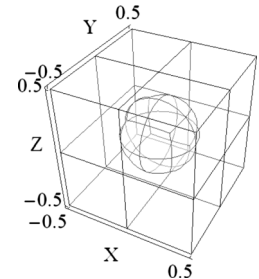


Fig. 1 a Macrostructure: system, load and expected result. b Porous microstructure: geometry and material data

scale FE² analysis. The system, load and material data are given in Fig. 1. A. For microscale analysis are standard linear and quadratic Lagrange (H1 and H2) finite elements and isogeometric finite elements with linear and quadratic Bezier splines (ISOB1 and ISOB2) chosen to show that in the case of homogeneous microstructure the results obtained with FE² analysis do not depend on the element formulation on micro level. Hence, homogeneous RVE was discretized with a $2 \times 2 \times 2$ finite elements mesh for linear formulations and with a single element mesh for quadratic formulations. Size of RVE does not affect the resulting microstress field or its derivatives in FE² analysis. The load was applied in ten equal load steps. The resulting displacements of point P (see Fig. 1) obtained with different FE² formulations are compared to the results of single scale analysis. The results presented in Table 1 show that in case of homogeneous microstructure all two-scale FE² analyses give numerically the same results as single scale analysis within machine precision accuracy.

7.2 Numerical efficiency consideration of proposed FE² formulation

A computational homogenisation example of porous material is considered to justify the proposed FE² formulation in terms of numerical efficiency. Here the performance of conventional FE² formulation with asymmetric deformation gradient as strain measure is compared to proposed FE² formulation with symmetric stretch tensor as strain measure. Macrostructure is a Cooke membrane and microstructure is represented by a cubic RVE with spherical opening in its center. Volume fraction of spherical opening is 0.1 %. The system, load and material data are given in Fig. 1. Cooke membrane is on macro level discretized with a mesh of

Table 1 Vertical displacement of point P in a homogeneous Cooke membrane test for single scale analysis and different two-scale FE² analyses

Single scale analysis					
Displ. w_S	36.6261 mm				
Two-scale FE ² analysis					
	H1	H2	ISOB1	ISOB2	
RVE DOF	93	93	93	93	
Displ. w_M (mm)	36.6261	36.6261	36.6261	36.6261	
$ w_S - w_M $	4.974×10^{-14}	4.974×10^{-14}	4.263×10^{-14}	5.684×10^{-14}	

Table 2 Vertical displacement of point P (w_P) and computational times for one Newton–Raphson iteration in a porous Cooke membrane test

Microscale (RVE)				Macroscale	
Element	Mesh	DOF	Memory (MB)	w_P (mm)	Time (s)
Conventional FE ² formulation					
H1	6 · (4 × 4 × 4)	1608	12.1	42.4457	53
	6 · (8 × 8 × 8)	11028	145.3	43.0747	1047
ISOB2	6 · (2 × 2 × 2)	738	9.0	43.1024	62
	6 · (4 × 4 × 4)	2964	63.1	43.2581	481
H2	6 · (2 × 2 × 2)	1608	17.6	43.1135	75
	6 · (4 × 4 × 4)	11028	198.2	43.3050	1254
New FE ² formulation					
H1	6 · (4 × 4 × 4)	1608	12.0	42.4457	44
	6 · (8 × 8 × 8)	11028	144.7	43.0747	867
ISOB2	6 · (2 × 2 × 2)	738	8.9	43.1024	45
	6 · (4 × 4 × 4)	2964	62.9	43.2581	360
H2	6 · (2 × 2 × 2)	1608	17.3	43.1135	62
	6 · (4 × 4 × 4)	11028	187.3	43.3050	1011

For RVE analysis various finite element formulations were used

4 × 1 × 4 standard linear Lagrange (H1) finite elements. Computational model of cubic RVE is composed of six equal patches, each of them is associated to one RVE boundary plane and one sixth of spherical opening in the center of RVE (see Fig. 1). Each of these six equal patches is discretized with standard linear (H1) and quadratic (H2) Lagrange finite elements and quadratic isogeometric finite elements (ISOB2) and quadratic standard Lagrange finite elements (H2) for several mesh densities (see Table 2). The load was applied in ten equal load steps. The resulting vertical displacement of point P (see Fig. 1) obtained with conventional and new FE² formulation together with associated computational time per one Newton–Raphson iteration on macro level is shown in Table 2. When compared to conventional FE² formulation, the proposed FE² formulation makes an additional calculation and linearisation of a tensor square root in macroanalysis which increases evaluation time. On the other hand, less complex boundary conditions related sensitivity analysis of RVE in the proposed FE² formulation reduces global tangent matrix evaluation time. Obtained total reduction of average

CPU time for this particular example varies between 17 and 27 % for one Newton–Raphson iteration on macroscale (see Table 2). CPU time is most reduced in the case of isogeometric microanalysis, which also exhibits most favorable ratio between accuracy and computational cost (CPU time and memory) for the coarsest RVE mesh. Reduced amount of needed memory space is also noted (see Table 2).

The convergence of FE² analysis is then studied with mesh refinement on macro scale. RVE mesh has a fixed size of 6 · (2 × 2 × 2) finite elements. Quadratic isogeometric finite elements (ISOB2) were used for microanalysis and quadratic standard Lagrange finite elements (H2) for macroanalysis. The convergence of the resulting macroscopic displacement w_P is shown in Fig. 2 with regard to number of macroscopic degrees of freedom (DOF).

The effect of volume fraction of openings on resulting vertical displacement w_P is presented next. The porosity was increased to the point where the first opening closes at maximal load (further increase of porosity was not possible since self contact was not considered in finite element formula-

Fig. 2 Convergence of vertical displacement of point P (w_P) in a porous Cooke membrane test with increasing of macroscopic finite element mesh density (degrees of freedom—DOF)

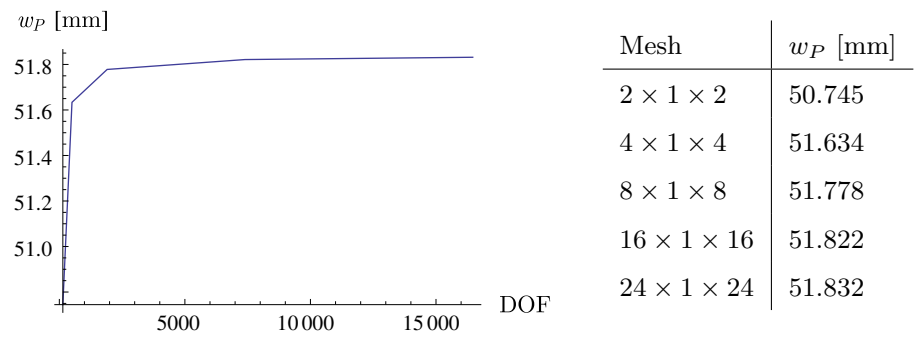
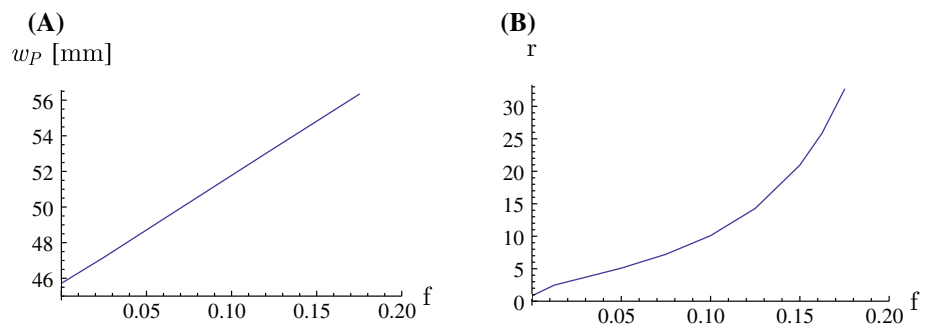


Fig. 3 a Vertical displacement of point P (w_P) and **b** ratio (r) between maximal calculated microscopic and macroscopic Mises stress in a porous Cooke membrane test with regard to volume fraction of openings (f)



tion). Figure 3 shows that the resulting vertical displacement w_P increases proportional to volume fraction of the openings while the ratio between maximal microscopic and maximal macroscopic Mises stress tends to increase exponentially. The point of maximal macroscopic Mises stress is approximately at maximal tension at the top of constrained end. Maximal microscopic Mises stress was located at the bottom of the Cooke’s membrane in nodes located from 24 mm to 27 mm away from constrained end and being closer to constrained end for higher values of f .

7.3 Agreement between numerical and analytical estimates for effective elastic stiffness tensor

Accuracy of the presented FE² procedure is tested on a computational homogenisation example of porous linear elastic material. Linear elastic material is chosen to stand comparison to known analytical solution for effective elastic stiffness tensor C_{eff} estimate derived by Nemat-Nasser ([11–13]). Due to linear elasticity the presented FE² procedure is simplified. Instead of stretch tensor \mathbf{U} small strain deformation tensor $\mathbf{E} = \frac{1}{2}(\mathbf{H} + \mathbf{H}^T)$ is applied and its six independent components are used for sensitivity analysis. Strain density function is given by $W(\mathbf{E}) = \frac{\lambda}{2}(\text{tr}(\mathbf{E}))^2 + \mu \text{tr}(\mathbf{E}^2)$ and stress tensor is defined by $\mathbf{S} = \hat{\delta}W/\hat{\delta}\mathbf{E}$. Macrostructure is a cube with dimensions 10 mm × 10 mm × 10 mm with fixed clamped end condition on one side and a prescribed uniform displacement $u = 1$ mm on the opposite side. The microstructure is represented by a linear elastic cube (RVE) with spherical opening in its center. Volume

fraction of spherical opening is 0.1 %. Geometry of RVE is given in Fig. 1. B. Macroscale analysis is preformed by one standard linear Lagrange (H1) finite element. On micro level, different element definitions and mesh densities are used for accuracy and efficiency comparison of the considered finite element formulations. An objective mesh of a sphere is composed of six equal patches, as described in example 7.2. The exact geometry of the considered quadratic surface can only be represented by quartic Bezier splines (see [29,30]). Hence, the chosen isogeometric FE² procedure for this numerical homogenisation example performs microanalysis with isogeometric finite elements with quartic Bezier splines (ISOB4). The results were obtained also for standard FE² procedures that analyze microstructure with standard linear and quadratic Lagrange (H1 and H2) finite elements. The numerical solutions for components of effective elastic stiffness tensor

$$C_{eff} = \begin{bmatrix} \bar{C}_{1111} & \bar{C}_{1122} & \bar{C}_{1122} & 0 & 0 & 0 \\ & \bar{C}_{1111} & \bar{C}_{1122} & 0 & 0 & 0 \\ & & \bar{C}_{1111} & 0 & 0 & 0 \\ & & & \bar{C}_{2323} & 0 & 0 \\ \text{symm.} & & & & \bar{C}_{2323} & 0 \\ & & & & & \bar{C}_{2323} \end{bmatrix} \quad (29)$$

of porous linear elastic material with associated computational time are given in Table 3 for various RVE mesh densities and all considered FE² formulations. One iteration of Newton–Raphson method returns converged solution

Table 3 Convergence of \bar{C}_{ijkl}/C_{ijkl} ratios for effective elastic stiffness tensor C_{eff} evaluated with isogeometric and standard FE² procedures and associated total computational time

Microscale (RVE)		Macroscale			
Mesh	DOF	\bar{C}_{1111}/C_{1111}	\bar{C}_{1122}/C_{1122}	\bar{C}_{2323}/C_{2323}	Time (s)
H1 microanalysis					
6 · (4 × 4 × 4)	1608	0.82088	0.76857	0.83581	4
6 · (8 × 8 × 8)	11,028	0.80530	0.75058	0.81882	39
6 (16 × 16 × 16)	78438	0.80110	0.74588	0.81387	1380
H2 microanalysis					
6 · (2 × 2 × 2)	1608	0.80389	0.74741	0.81665	7
6 · (4 × 4 × 4)	11,028	0.79999	0.74451	0.81266	60
6 · (8 × 8 × 8)	78,438	0.79969	0.74431	0.81217	1645
ISOB4 microanalysis					
6 · (1 × 1 × 1)	1608	0.80061	0.74460	0.81560	13
6 · (2 × 2 × 2)	2964	0.79974	0.74423	0.81241	66
6 · (4 × 4 × 4)	7566	0.79965	0.74426	0.81212	495

with machine precision since it is a linear problem. FE² analysis converges to same solutions for all considered FE² formulations, where isogeometric FE² formulation exhibits highest convergence rate and superior numerical efficiency of FE² analysis in terms of most favorable ratio between solution accuracy and computational time. This result confirms that exact modeling of microstructure geometry produces superior results of numerical homogenisation procedure. The obtained numerical solutions are compared to Nemat-Nassers analytical solution for effective elastic stiffness tensor estimate C_{eff} of periodic multiphase linear elastic materials (see [11]). Nemat-Nasser assumed in all directions infinite periodic, linear elastic and isotropic microstructure and derived a Fourier series expansion of displacement and stress fields. If RVE is a cube with boundary size a and spherical opening of radius b , effective elastic stiffness tensor C_{eff} of periodic porous linear elastic material is estimated as

$$C_{eff} = C \left(\mathbf{1} - f (\mathbf{1}^{(4s)} - S^p)^{-1} \mathbf{1}^{(4s)} \right), \tag{30}$$

where $\mathbf{1}^{(4s)}$ is fourth order symmetric unit tensor and S^p reference elastic stiffness tensor. Tensor S^p has cubic symmetry like C_{eff} (see (29)) and its nonzero components are written as

$$S_{1111}^p = \sum_{\mathbf{v} \neq \mathbf{0}} \sum \sum f g(\mathbf{v})^2 (v_1/|\mathbf{v}|)^2, \tag{31}$$

$$\mathbf{v} = \pi/a (v_1, v_2, v_3), v_i \in \mathbb{Z} \quad \forall i$$

$$S_{1122}^p = \sum_{\mathbf{v} \neq \mathbf{0}} \sum \sum f g(\mathbf{v})^2 (v_1/|\mathbf{v}|)^4, \tag{32}$$

$$S_{2323}^p = \sum_{\mathbf{v} \neq \mathbf{0}} \sum \sum f g(\mathbf{v})^2 (v_2/|\mathbf{v}|)^2 (v_3/|\mathbf{v}|)^2, \tag{33}$$

where $|\mathbf{v}|$ is Euclidian norm of vector \mathbf{v} , f volume fraction of spherical opening and

Table 4 Convergence of \bar{C}_{ijkl}/C_{ijkl} ratios for Nemat-Nassers analytical estimate of C_{eff} with associated computation time

n	\bar{C}_{1111}/C_{1111}	\bar{C}_{1122}/C_{1122}	\bar{C}_{2323}/C_{2323}	Time (s)
100	0.800784	0.746139	0.812918	2
500	0.799953	0.74474	0.812323	237
1000	0.799848	0.744563	0.812248	1892

$$g(\mathbf{v}) = 3 (\sin(b |\mathbf{v}|) - b |\mathbf{v}| \cos(b |\mathbf{v}|)) / (b |\mathbf{v}|)^3 \quad \text{for } |\mathbf{v}| \neq 0. \tag{34}$$

Analytical estimates for C_{eff} of considered periodic porous linear elastic material are calculated for $v_i \in \{-n, n\} \quad \forall i \in \{1, 2, 3\}$ and various values of n and presented in Table 4. All calculated numerical solutions in Table 3 and analytical estimates converge to same solution which validates the accuracy of the presented FE² implementation. The C code for evaluation of Nemat-Nassers C_{eff} estimate is generated by AceGen so that computation time can be compared to the computation time of the presented FE² procedure. Evaluation of Nemat-Nassers analytical estimate gives solution with three correct digits in 237 seconds, whereas the standard FE² procedure that performs microanalysis with standard quadratic Lagrange element (H2) achieves this in 60 seconds and isogeometric FE² procedure in 66 seconds.

8 Conclusions

This paper presents a new FE² formulation that significantly reduces the computational cost of two-scale FE² analysis, proves its compliance to energy averaging theorem and discusses its consistency, accuracy and numerical efficiency on numerical homogenisation examples. The new FE² for-

mulation introduces symmetric stretch tensor as a macro strain measure instead of conventionally used asymmetric deformation gradient to determine the prescribed boundary conditions of underlying microstructure (RVE). This reduces the computational cost of boundary conditions related sensitivity analysis of RVE that is performed on micro level to evaluate the local macroscopic tangent operator. Stretch tensor is matrix square root of Cauchy–Green tensor which is evaluated together with its first and second derivatives with automatic differentiation of appropriate scalar generating function to avoid the difficulties associated with evaluation of matrix square root based on polar decomposition. The new two-scale FE^2 scheme was implemented in symbolic code generation system AceGen which automates derivation of quantities needed in primal and sensitivity analyses on micro level and primal analysis on macro level of FE^2 procedure and also simultaneously performs automatic differentiation and optimization of expressions. The FE^2 flowchart based on AceGen enables objective comparison of different FE^2 formulations. Various FE^2 formulations with isogeometric and standard finite element microanalysis were developed and tested on numerical homogenisation examples to study consistency, accuracy and numerical efficiency of FE^2 analysis. Consistency of micro–macro coupling is first tested on a homogeneous material. Results obtained with FE^2 analysis and single scale FEM analysis are numerically identical with machine precision for all considered FE^2 formulations. New FE^2 formulation was further tested on homogenisation of a porous hyperelastic material. Results obtained with conventional and new FE^2 formulation show that introduction of symmetric stretch tensor as a strain measure contributes to a total reduction of computation time between 17 and 27 % depending on chosen finite element formulation for microanalysis. Reduced sensitivity analysis lowers also memory usage during calculation. Accuracy of the presented FE^2 formulation is further verified on numerical homogenisation of linear elastic porous material for which Nemat-Nasser (see [11]) derived an analytical estimate of effective elastic stiffness tensor. All considered isogeometric and standard FE^2 procedures converge in both numerical examples to same converged values and in latter example to Nemat-Nassers analytical estimate. The obtained results confirm better convergence rate regarding number of degrees of freedom for higher order isogeometric FE^2 analysis and show comparable numerical efficiency in terms of most favorable ratio between solution accuracy and computational time of higher order isogeometric FE^2 analysis when compared to standard FE^2 analysis with quadratic Lagrange finite elements.

Acknowledgments The financial support for this work was obtained from the Slovenian Research Agency within the PhD Grant Agreement No: 1000-09-310290.

References

1. Feyel F (1999) Multiscale FE^2 elastoviscoplastic analysis of composite structures. *Comput Math Sci* 16:344–354
2. Kouznetsova V, Brekelmans WAM, Baaijens FPT (2001) An approach to micro–macro modeling of heterogeneous materials. *Comput Mech* 27:37–48
3. Michel JC, Moulinec H, Suquet P (1999) Effective properties of composite materials with periodic microstructure: a computational approach. *Comput Methods Appl Mech Eng* 172:109–143
4. Miehe C, Koch A (2002) Computational micro-to-macro transition of discretized microstructures undergoing small strain. *Arch Appl Mech* 72:300–319
5. Miehe C, Schotte J, Schröder J (1999) Computational micro–macro transitions and overall moduli in the analysis of polycrystals at large strains. *Comput Math Sci* 16:372–382
6. Miehe C, Schröder J, Becker M (2002) Computational homogenization analysis in finite elasticity: material and structural instabilities on the micro- and macro-scales of periodic composites and their interaction. *Comput Methods Appl Mech Eng* 191:4971–5005
7. Terada K, Hori M, Kyoya N, Kikuchi N (2000) Simulation of multi-scale convergence in computational homogenization approaches. *Int J Solids Struct* 37:2285–2311
8. Lamut M, Korelc J, Rodič T (2011) Multiscale modelling of heterogeneous materials. *Materiali in tehnologije* 45:421–426
9. Temizer I, Wriggers P (2008) On the computation of the macroscopic tangent for multiscale volumetric homogenization problems. *Comput Methods Appl Mech Eng* 198:495–510
10. Korelc J (2009) Automation of primal and sensitivity analysis of transient coupled problems. *Comput Mech* 44(5):631–649
11. Nemat-Nasser S, Hori M (1999) *Micromechanics: overall properties of heterogeneous materials*, 2 rev edn. Elsevier, Amsterdam
12. Nemat-Nasser S, Taya M (1981) On effective moduli of an elastic body containing periodically distributed voids. *Q Appl Math* 39:43–59
13. Nemat-Nasser S, Taya M (1985) On effective moduli of an elastic body containing periodically distributed voids: comments and corrections. *Q Appl Math* 43:187–188
14. Bonet J, Wood RD (2008) *Nonlinear continuum mechanics for finite element analysis*. Cambridge University Press, Cambridge
15. Jia L (2004) Exact expansions of arbitrary tensor functions $f(a)$ and their derivatives. *Int J Solids Struct* 41(2):337–349
16. Goddard JD, Ledniczky K (1997) On the spectral representation of stretch and rotation. *J Elast* 47(3):255–259
17. Korelc J, Stupkiewicz S (2014) Closed-form matrix exponential and its application in finite-strain plasticity. *Int J Numer Meth Eng* 98:960–987
18. Khisaeva ZF, Ostoja-Starzewski M (2006) On the size of rve in finite elasticity of random composites. *J Elast* 85:153–173
19. Hill R (1965) A self-consistent mechanics of composite materials. *J Mech Phys Solids* 13:213–222
20. Hill R (1984) On macroscopic effects of heterogeneity in elastoplastic media at finite strain. *Math Proc Camb Philos Soc* 95:481–494
21. Kouznetsova V (2002) *Computational homogenization for the multiscale analysis of multi-phase materials*. Ph.D. thesis, Eindhoven University of Technology
22. Wolfram Research Inc., *Mathematica 9 manual*
23. Korelc J, Wriggers P (2008) *Automation of the finite element method*. Springer, Berlin
24. Korelc J (1997) Automatic generation of finite-element code by simultaneous optimization of expressions. *Theor Comput Sci* 187(1–2):231–248

25. Bartholomew-Biggs M, Brown S, Christianson B, Dixon L (2000) Automatic differentiation of algorithms. *J Comput Appl Math* 124(1–2):171–190
26. Bischof C, Hovland P, Norris B (2002) Implementation of automatic differentiation tools. In: Proceedings of the ACM SIGPLAN workshop on partial differentiation and semantics-based program manipulation
27. Griewank A (2000) Evaluating derivatives: principles and techniques of algorithmic differentiation. SIAM, Philadelphia
28. Cottrell J, Hughes TJR, Bazilevs Y (2009) Isogeometric analysis. Wiley, Chichester
29. Hoschek J, Dietz R, Jüttler B (1995) Rational patches on quadric surfaces. *Computer-Aided Des* 27(1):27–40
30. Farin G (1999) Nurbs curves and surfaces: from projective geometry to practical use, 2nd edn. A. K. Peters Ltd, Natick